Sensors and Materials, Vol. 34, No. 11 (2022) 3967–3987
MYU Tokyo

S & M 3090

Multi-objective Optimization of Non-invasive Voltage Sensor Considering Sensitivity, Array Arrangement, and Cost

Qi Qian,[1] Liang Shu,[1*] Linghao Wang,[1] and Zhizhou Bao[2]

[1]Low Voltage Apparatus Technology Research Center of Zhejiang, College of Electrical and Electronic Engineering, Wenzhou University, Wenzhou 32500, China
[2]Zhejiang People Electric Co., Ltd., Wenzhou 325000, China

(Received September 14, 2022; accepted October 18, 2022)

Keywords: non-invasive voltage sensor, electrode array, array design, multi-objective optimization

Non-invasive sensors are designed to offer ease of installation and avoid contact with dangerous hot wires. To optimize the array design of sensors, a multi-objective optimization method considering sensitivity, array arrangement, and cost is proposed in this study. The total array induced charge Q and the location sensitivity S_1 are established to evaluate the sensor performance. On the basis of these evaluation indexes, design criteria for the array arrangement are proposed, which include the electrode shape, the array profile, and the space interval angle between electrode elements. Following this design basis, two objective functions for the array design are investigated. The first objective function is based on the entropy-CRITIC weight of the two regression models and the second objective function is based on the manufacturing cost. For the multi-objective design, the NAGA-II algorithm is employed and the VIKOR strategy is used to select the decision from the Pareto set. Optimization results show that, compared with the original design, the value of the first objective function is improved by 74.35% and the value of the second objective function is reduced by 22.99%. It is found that the rectangular shape is suitable for the single-electrode element design. The sensing array is best designed in a ring profile, and the optimal number of electrodes is 3.

1. Introduction

Voltage sensing is one of the basic measurement techniques of modern power systems and is used in residential, industrial, and utility applications.(1) The measurement of voltages in a cable enclosed in a structure is a challenging task but with great potential applications. In the traditional way of measuring voltage, direct contact with the metal conductor in cables is required, which is difficult and unsafe. Thus, researchers have been developing non-invasive methods of measuring voltage,(2,3) which estimate the cable voltage using harvested electric field energy. Non-invasive sensors offer ease of installation and avoid contact with dangerous hot wires.

The principle of a non-invasive voltage sensor(4,5) is to convert the induced charge of the electrode in the sensor into induced voltage. The design parameters of the induced electrode can

*Corresponding author: e-mail: shu22@wzu.edu.cn
https://doi.org/10.18494/SAM4104

ISSN 0914-4935
https://myukk.org/

directly affect the voltage measurement results. In Refs. 6 and 7, a voltage sensor with a single electrode was developed, which calculated the voltage of the cable by measuring the electric field at a fixed position around the cable. However, a single electrode cannot adequately describe the spatial field distribution and thus limits the overall sensing performance. To overcome this problem, researchers are developing sensors based on multiple electrode array designs. In Ref. 8, a capacitive probe with two sensor heads was implemented, and the dual-electrode probe was placed on only one side of the cable. This placement may have affected the sensing performance since the field distribution on the other side could not be detected. In Ref. 9, a novel electrode array composed of four uniformly distributed electrodes was developed to collect the spatially distributed electric field around a power cable. In Ref. 10, a spherical sensor with six electrodes was proposed to decrease the measurement error caused by angular deflection. In Ref. 11, an array of magnetic field sensors was used to measure AC currents in a bundle of inaccessible, enclosed conductors. The array-based non-invasive sensor was able to obtain the spatially distributed field and hence improve the sensor performance. An optimal array design includes the optimal design of the single-electrode shape, the electrode quantities, and the overall array arrangement. However, such optimal array design of non-invasive voltage sensors has hardly been discussed.

Electrode array optimization is different from the existing optimal sensor placement (OSP) problem.[12] OSP is usually discussed in areas such as structural health monitoring (SHM),[13] load identification,[14] and response reconstruction.[15] The objective of OSP is to determine the most suitable sensor placement to obtain comprehensive response information, such as the structural health, load, or vibration of a structure, using very few sensors. Intelligent optimization algorithms such as the genetic algorithms[16,17] and monkey algorithm[18] are usually used to solve such problems. In Ref. 19, using a genetic algorithm, the OSP for deployable antenna module health monitoring in space solar power satellites was proposed. Similar research was reported in Ref. 20, in which the optimal number of sensors was suggested and the corresponding optimum locations were found by using the genetic algorithm and a proposed strategy for determining the number and placement of sensors. Unlike OSP, we aim to improve the overall performance of non-invasive voltage sensors by suitably designing the electrode array.

It is desirable to develop sensors with very high accuracy, high stability, and a reasonable manufacturing cost. Toward achieving these aims, in this study, we propose a multi-objective optimization method for non-invasive voltage sensors considering sensitivity, array arrangement, and cost. Electrode array evaluation indexes are first established to evaluate the sensor performance, including the total array induced charge Q and location sensitivity S_1. The location sensitivity is mainly defined to investigate the sensing stability when the relative locations between a hot wire and the array are changing. On the basis of such indexes, we discuss the array design including the electrode shape, the array profile, and the space interval angle between electrode elements. We investigate two objectives for the array design: the optimal sensing performance and a reasonable cost. For the first objective, two regression models are developed corresponding to Q and S_1. The objective function is then constructed on the basis of the entropy-CRITIC weight of the two regression models. For the second objective, the objective

function is built according to the manufacturing cost of the electrode element and the number of elements. For the multi-objective design, the NAGA-II algorithm is employed to optimize the problem, and the VIKOR strategy is used to finally select the decision from the Pareto set.

The paper is organized as follows. The non-invasive voltage model and the sensing principle are introduced in Sect. 2. In Sect. 3, the design criteria for the array arrangement are presented. The proposed multi-objective functions are described in Sect. 4, which is followed by the optimization solution and case analysis in Sects. 5 and 6, respectively. Conclusions are given in Sect. 7.

2. Non-invasive Voltage Measurement

2.1 Principle of non-invasive voltage sensing

A typical non-invasive voltage sensor, including the electrode array, the sensing area, and the corresponding fixtures, is depicted in Fig. 1. When a powered cable passes through the sensing area, the intensity of the stray electric field around the cable is determined from the cable voltage using only a quasi-static approximation. Therefore, it is possible to estimate the line voltage using the harvested electric field energy. Charge is induced on the surface of the array electrodes. By measuring the charge on the inducted electrode, the cable voltage can be measured non-invasively.

According to the principle of electrostatic induction, an induced charge q is generated on a metal electrode's surface when the electrode is placed in a time-varying electric field. The current generated by the changing charge flows through the grounding resistance R_m, producing a voltage drop, and the relationship can be described by

$$q = \oint_{A_0} \varepsilon_0 E_0 dA_0 = \varepsilon_0 E_0 A_{eq}, \tag{1}$$

$$V_0(t) = R_m \frac{dq}{dt} = \varepsilon_0 A_{eq} R_m \frac{dE_0}{dt}, \tag{2}$$

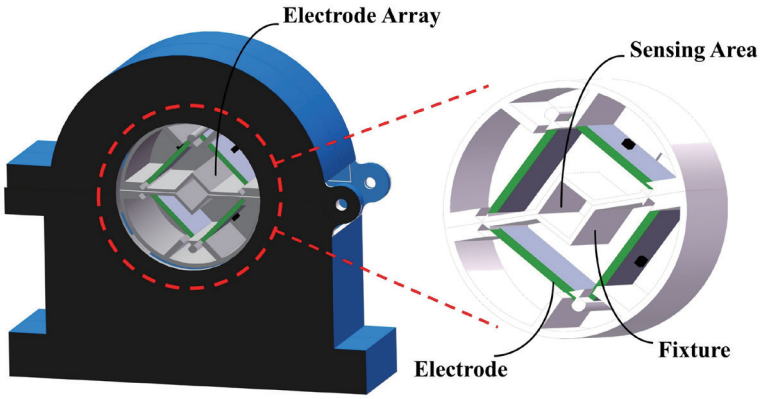

Fig. 1. (Color online) Model of the non-invasive voltage sensor.

where q is the induced charge of the electrode, ε_0 is the vacuum permittivity, E_0 is the electric field strength, A_0 is the electrode surface area, R_m is the grounding resistance, and V_0 is the voltage drop. The relationship between the cable voltage and electric field strength is expressed by

$$\varphi_0 = \frac{1}{F} \cdot E_0, \tag{3}$$

where φ_0 is the cable voltage and F is the scale factor, which is determined by the relative positions of the electrode and the cable. From Eqs. (2) and (3), φ_0 can be described in terms of V_0 as

$$\varphi_0 = \frac{\int_0^t V_0 dt}{\varepsilon_0 A_{eq} R_m F}. \tag{4}$$

Based on this relationship, the non-invasive measurement of the cable voltage can be realized if the voltage drop V_0 is collected.

2.2 Electrode array evaluation index

The array arrangement and the array parameters are key factors that can affect the sensing performance. Optimization of the electrode array includes the design of the electrode shape, the array profile, and the space interval angle between electrode elements. For each electrode element, it is also necessary to understand how the sensing performance is affected by the electrode area, the electrode thickness, and the number of electrodes. To implement the optimal design, the evaluation indexes must first be set up. From Eq. (2), the induced voltage is directly determined by the total amount of charge. The measurement performance and cable voltage are reflected in the total charge. The total array induced charge Q is chosen as one of the evaluation indexes, which is calculated as

$$Q = \frac{\sum_{i=1}^{n} \sum_{j=1}^{m} q_{ij}}{m}, \tag{5}$$

where n is the number of electrodes in the array, m is the number of measurements when the cable is placed at different locations in the sensing area, and q_{ij} is the induced charge of a single-electrode element.

From Fig. 1, it can be observed that the relative distance between the cable and the electrode array can differ if the diameter of the cable that passes through the sensor varies when the rated current level varies. The induced voltage may change with the relative location. In such a case,

the sensor should be designed so that the voltage is unlikely to change with the relative location, resulting in reliable sensing results. To reflect this requirement, here, we assume that if the cable is moved from location j to the next location $j + 1$, the location sensitivity S_1 can be defined as the evaluation index to investigate the sensing reliability. S_1 is defined as

$$S_1 = \frac{\left|Q_{j+1} - Q_j\right|}{Q_j}, \tag{6}$$

where Q_j represents the total array induced charge at location j. From Eq. (6), a low value of S_1 indicates a reliable sensing performance.

3. Design Criteria for Array Arrangement

The sensing performance of the array is affected by its arrangement. We carry out simulations to analyze the sensing performance in terms of the total array induced charge Q and the location sensitivity S_1 for different electrode shapes, array profiles, and space intervals between the electrode elements.

3.1 Effect of electrode shape

The single-electrode shape must first be determined by comparing the induced charge q for different electrode shapes, which is calculated using Eq. (1), and its unit is C^{-12} because the amount of induced charge q is small. Here, we compare rectangular and circular electrodes. To ensure the accuracy of the experimental results, the thickness of both electrodes is 0.3 mm, the electrodes are both placed parallel to the cable with a distance between them of 12 mm, the diameter of the cable is 4 mm, and the amplitude of the cable voltage is 220 V. Then, q and S_1 for the two electrodes with four areas are compared, and the results are shown in Table 1. For example, when the area of the electrode is 100 mm^2 and the electrode is rectangular, the induced charge q is 15.416 C^{-12}. It is found that the induced charge of the rectangular electrode is 12.23% higher than that of the circular electrode, whereas the location sensitivity of the rectangular electrode is 1.1% lower than that of the circular electrode. Therefore, the rectangular shape is selected for the electrode.

3.2 Effects of electrode length and width

For the rectangular electrode, the length of the side parallel to the cable axis is defined as L and the width in the other direction is defined as W_L, as shown in Fig. 2. To determine the effects of the electrode length and width, two groups of electrodes are set up, one to analyze the effect of the length and the other to analyze the effect of the width. The initial size of the rectangular electrode is set as 10×10 mm^2. For the length group, the width W_L remains the same, and the induced charge Q_1 is calculated when the electrode length is increased from 10 to 20 mm. In the

Table 1
Comparison of rectangular and circular electrodes.

		Area/mm^2				Analysis
		100	144	196	256	
q/C^{-12}	Rectangular	15.416	22.235	30.430	40.225	Rectangular exceeds circular by 12.23%
	Circular	14.110	19.516	26.523	36.236	
$S_1 \times 100\%$	Rectangular	5.107	5.075	4.688	4.446	Rectangular is better than circular by 1.11%
	Circular	6.142	6.205	5.973	5.422	

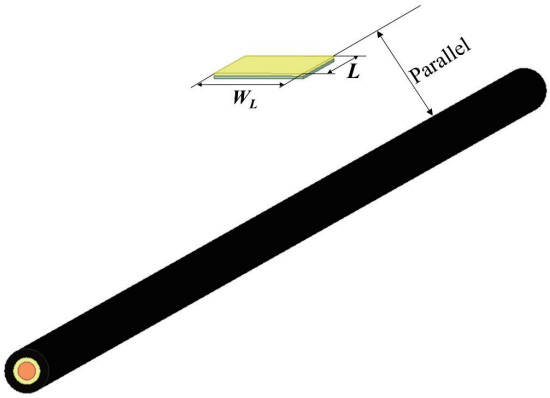

Fig. 2. (Color online) L and W_L of the rectangular electrode.

second group, the length L remains the same, and the induced charge Q_2 is calculated when the electrode width is increased from 10 to 20 mm. The charge ratio Q_1/Q_2 is calculated for each step increment of L or W_L, and the result is shown in Fig. 3. It can be seen that Q_1 is always larger than Q_2, which means that increasing L is more effective than increasing the induced charge. If the electrode area needs to be designed, it is better to change L than W_L.

3.3 Effect of array profile

The array profile is also an important factor affecting the sensing performance. Here, three different array profiles (side by side, square, and ring) are selected for comparison as shown in Fig. 4.

The cable voltage is 220 V. In each array profile, the number of electrode elements ranges from 3 to 8 and the total area of the electrode elements in the array remains unchanged. The evaluation indexes Q and S_1 are compared for the three different array profiles. To evaluate S_1, we assume that the cable follows the arrowed path shown in Fig. 5, in which there are 16 different locations. Q and S_1 are calculated using Eqs. (5) and (6), respectively. Comparisons of the three different array profiles are shown in Fig. 6, in which 3–8 electrode elements correspond to subplots (a)–(f). The conclusions of the comparison are given in Table 2. It can be seen that the ring profile demonstrates the best overall performance for the total induced charge Q, whereas the square profile demonstrates the best location sensitivity S_1. The side-by-side profile is not

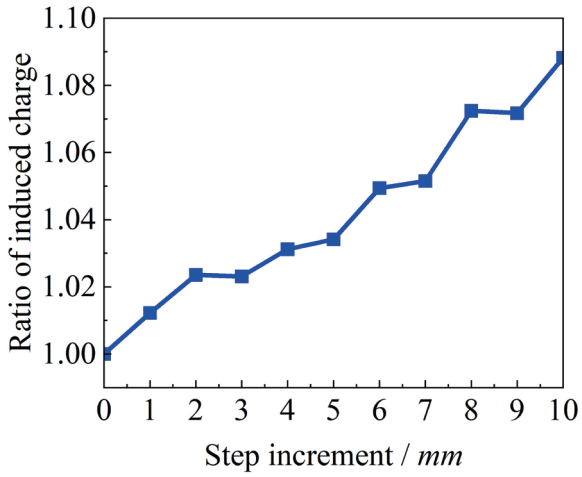

Fig. 3. (Color online) Effects of the length and width on the induced charge.

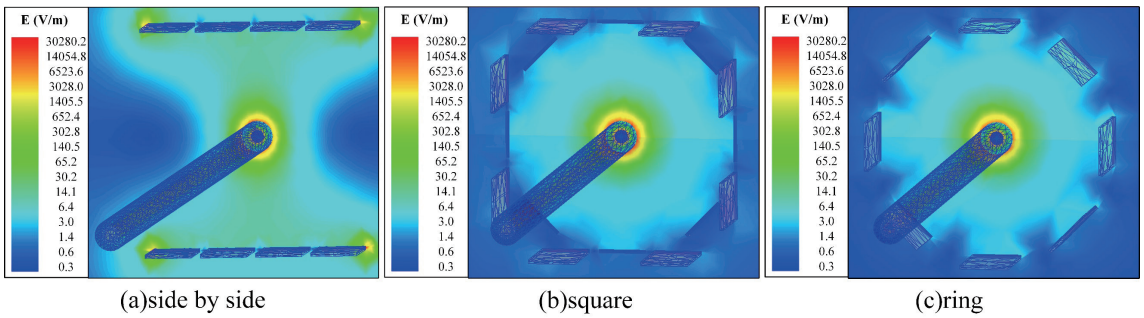

Fig. 4. (Color online) Three different array profiles.

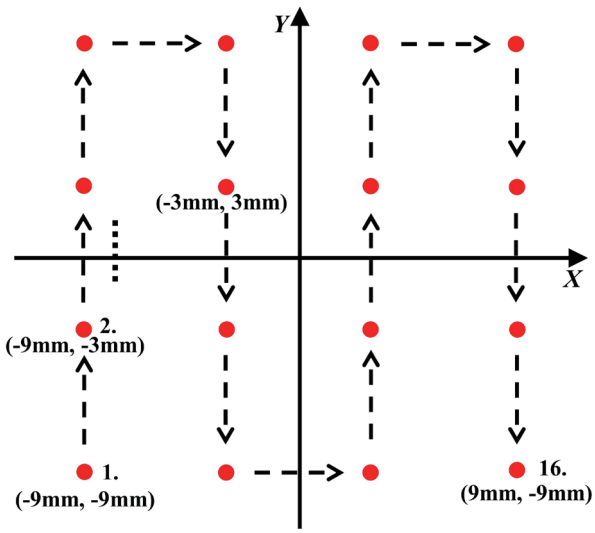

Fig. 5. (Color online) Moving path of cable.

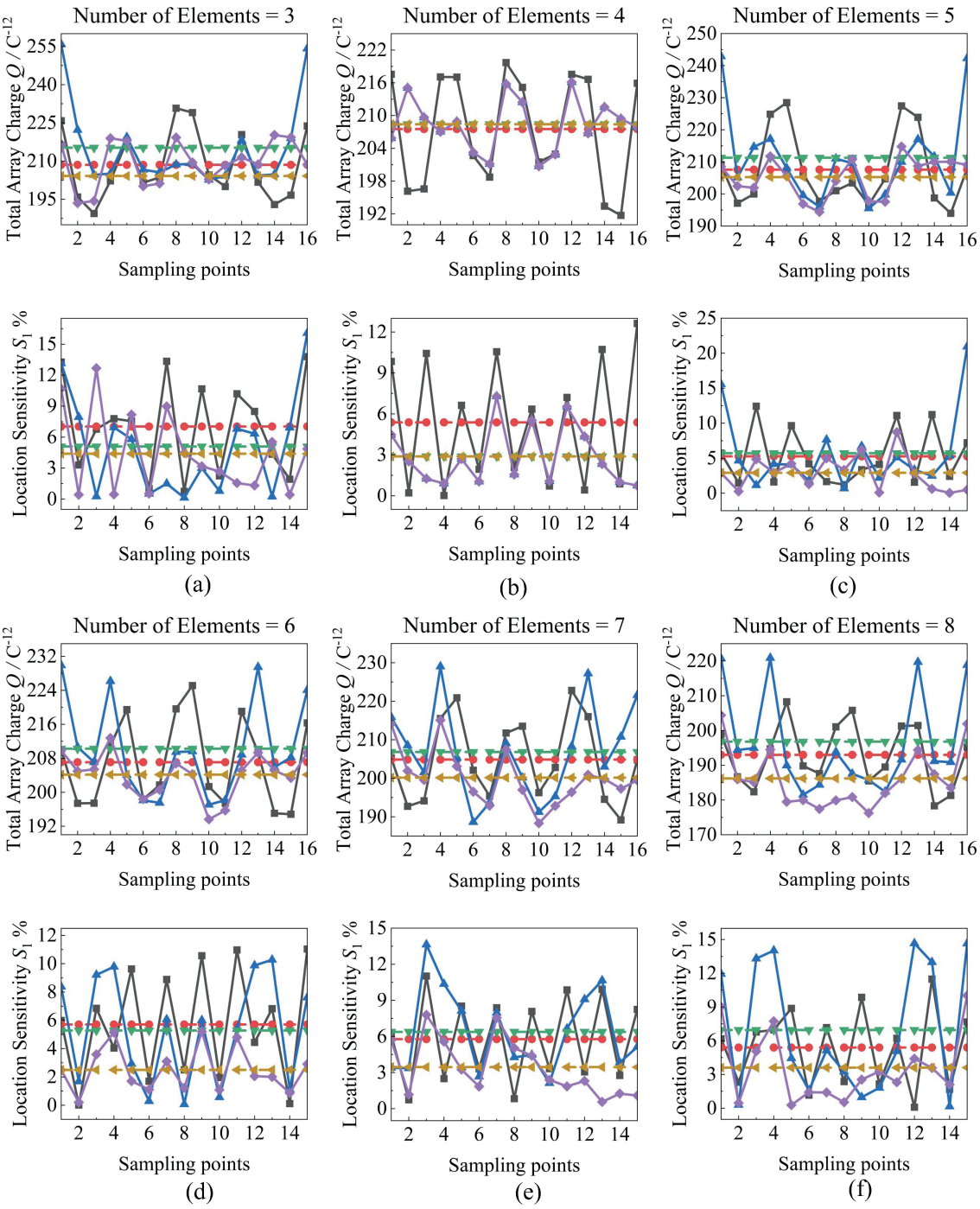

Fig. 6. (Color online) Sensing performance comparison of three different array profiles when the number of electrode elements ranges from 3 to 8.

recommended since it is produces poor values of both Q and S_1. Usually the voltage sensitivity is a very important factor in evaluating the sensor performance. Here, we select the ring profile for the sensor design.

Table 2
Comparison of evaluation indexes of the three different array profiles.

No.	Index	Performance sequence	Quantitative analysis	Select
3	Q/C^{-12}	Ring > square > side-by-side	Ring larger than square by 2.78% Ring larger than side-by-side by 3.23%	Ring
	S_1%	Square < ring < side-by-side	Square smaller than ring 0.69% Square smaller than side-by-side by 2.64%	
4	Q/C^{-12}	Ring = square > side-by-side	Ring equal to square Ring larger than side-by-side by 0.42%	Ring
	S_1%	Ring = square < side-by-side	Ring equal with square Ring smaller than side-by-side by 2.49%	
5	Q/C^{-12}	Ring > side-by-side > square	Ring larger than square by 2.93% Ring larger than side-by-side by 1.78%	Ring
	S_1%	Square < side-by-side < ring	Square smaller than ring by 2.34% Square smaller than side-by-side by 2.80%	
6	Q/C^{-12}	Ring > side-by-side > square	Ring larger than square by 2.99% Ring larger than side-by-side by 1.54%	Ring
	S_1%	Square < ring < side-by-side	Square smaller than ring by 2.78% Square smaller than side-by-side by 3.20%	
7	Q/C^{-12}	Ring > side-by-side > square	Ring larger than square by 3.33% Ring larger than side-by-side by 0.96%	Ring
	S_1%	Square < side-by-side < ring	Square smaller than ring by 2.92% Square smaller than side-by-side by 2.64%	
8	Q/C^{-12}	Ring > side-by-side > square	Ring larger than square by 5.68% Ring larger than side-by-side by 1.96%	Ring
	S_1%	Square < Side-by-side < ring	Square smaller than ring by 3.34% Square smaller than side-by-side by 1.78%	

3.4 Effect of space interval angle between electrode elements

The number of electrode elements in the ring-shaped array and the optimal space interval angle between them have an inverse relationship. Here, the effect of the space interval angle on the sensing performance is investigated. As shown in Fig. 7, the space interval angle is defined as the angle θ between electrode elements. Here, we vary the number of elements from 2 to 7 and calculate the total charge Q for different angles. The change in the electrode space interval angle is shown in Fig. 8, in which one of the elements is kept stationary and other elements rotate by a given angle while satisfying $\theta_1 = \theta_2$. The total charge Q is calculated until the front element reaches the element that is kept stationary. The results are shown in Fig. 9, in which the red dot-dashed lines are the fitted results showing the change in Q with the rotation angle. It can be seen that the optimal space interval angle is 180° when there are two elements. Similarly, the optimal angles for three to seven elements are 120, 90, 72, 60, and 51.4°, respectively, which means that the electrode elements in the sensing array should be uniformly distributed.

3.5 Summary

On the basis of the above analysis, the following design criteria are obtained:

(1) A rectangular electrode should be used. Moreover, the induced charge is more sensitive to the electrode length than the width.
(2) A ring shape is recommended for the array profile.
(3) When the array consists of multiple electrode elements, they should be distributed uniformly.

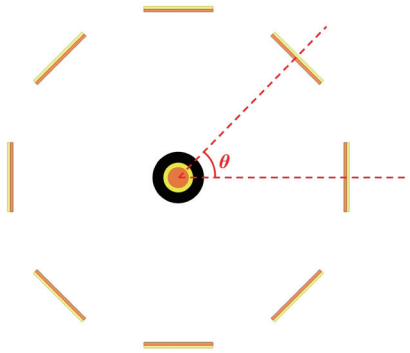

Fig. 7. (Color online) Space interval angle θ.

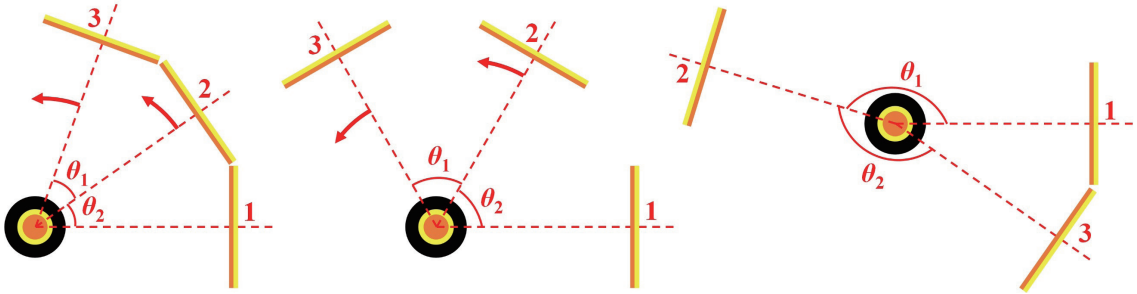

Fig. 8. (Color online) Change in electrode spacing of an array with three electrodes.

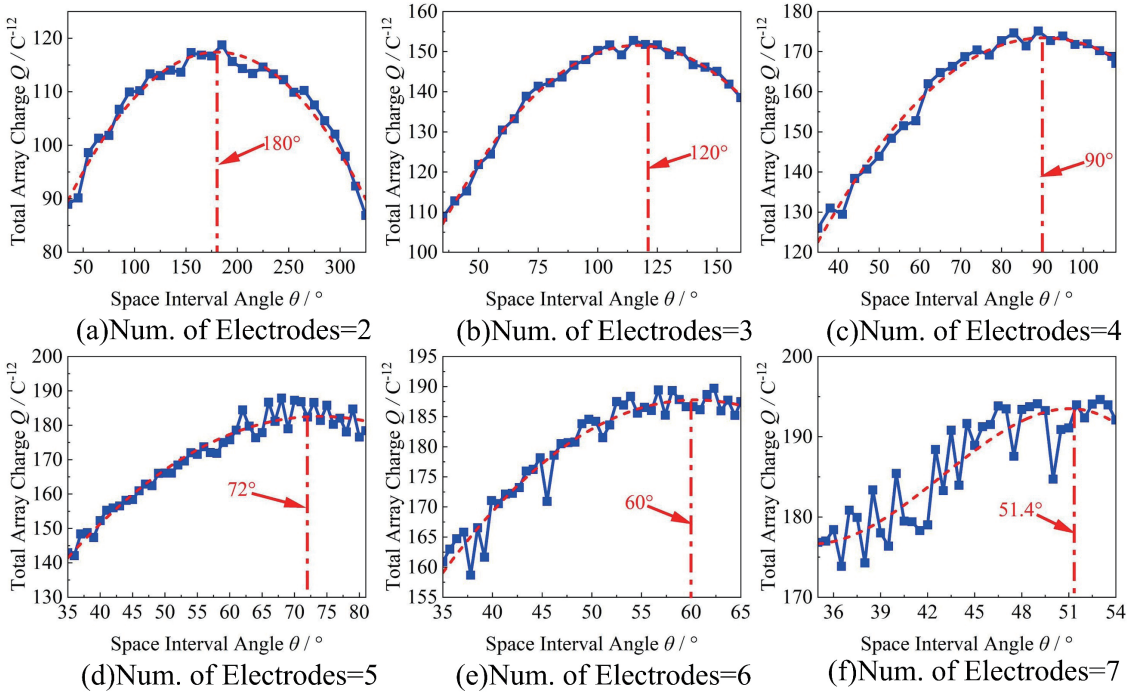

Fig. 9. (Color online) Relationship between space interval angle θ and charge Q.

4. Multi-objective Optimization

In Sect. 3, the evaluation indexes Q and S_1 were used to determine the electrode shape, the array profile, and the space interval angle between electrode elements. On the basis of these design criteria, the multi-objective optimization problem is discussed in this section. Usually, the total induced charge is larger if more electrode elements are used in the array. However, more elements result in a higher manufacturing cost. It is necessary to investigate the multi-objective optimization of the sensor array. Here, two objectives are discussed: the optimal sensing performance and a reasonable cost. For the first objective, two regression models are developed corresponding to Q and S_1. The objective function is then constructed on the basis of the entropy-CRITIC weight of the two regression models. For the second objective, the objective function is built according to the manufacturing cost of the electrode element and the number of elements.

4.1 Construction of multiple regression model

As shown in Fig. 10, several factors are considered in the model, including the number of electrode elements (factor A), the area of a single electrode (factor B), and the electrode thickness (factor C). We previously showed that the induced charge is more sensitive to the length than the width of the electrode. Thus, we change the area by changing the length L. It is assumed that the evaluation indexes Q and S_1 are dependent on factors A, B, and C. We use the multiple linear regression algorithm to investigate the relationship between the indexes and factors A, B, and C. The general expression of the model is

$$\boldsymbol{H}(\boldsymbol{X}) = \boldsymbol{X}\boldsymbol{W}$$
$$\boldsymbol{X} = \begin{bmatrix} x_{10} & x_{11} & \cdots & x_{1k} \\ x_{20} & x_{21} & \cdots & x_{2k} \\ \vdots & \vdots & \vdots & \vdots \\ x_{j0} & x_{j1} & \cdots & x_{jk} \end{bmatrix}, \boldsymbol{W} = \begin{bmatrix} w_0 \\ w_1 \\ \vdots \\ w_k \end{bmatrix}, \tag{7}$$

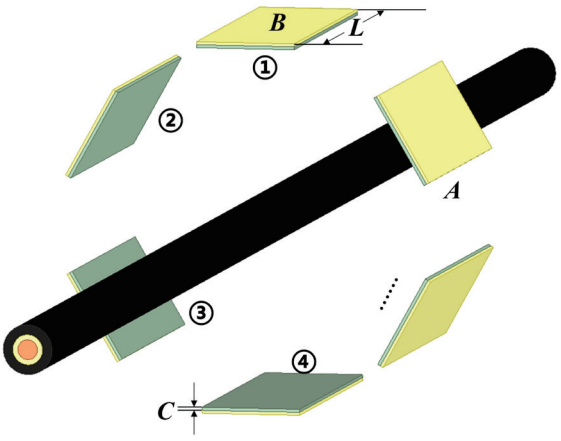

Fig. 10. (Color online) Array parameters.

where $\boldsymbol{H}(\boldsymbol{X})$ is the predictive value vector of the model, $\boldsymbol{X}$ is the input vector, and $\boldsymbol{W}$ is the regression coefficient vector.

The following loss function $J(\boldsymbol{W})$ is developed to quantify the prediction error:

$$J(\boldsymbol{W}) = \frac{1}{2}(\boldsymbol{XW} - \boldsymbol{Y})^T(\boldsymbol{XW} - \boldsymbol{Y}), \tag{8}$$

where $\boldsymbol{Y}$ is the objective value vector. When $J(\boldsymbol{W})$ is minimized, the optimal regression coefficient $\boldsymbol{W}$ is obtained from the following equation:

$$\frac{\partial J(\boldsymbol{W})}{\partial \boldsymbol{W}} = 0 \Rightarrow \boldsymbol{W} = (\boldsymbol{X}^T\boldsymbol{X})^{-1}\boldsymbol{X}^T\boldsymbol{Y}. \tag{9}$$

To improve the accuracy of the regression model, in addition to factors A, B, and C, the products of the pairs of factors are also added as the dependent variables. Thus, the input variables of the model are A, B, C, $A \times B$, $A \times C$, and $B \times C$, corresponding to x_1, …, x_6 in the input vector, respectively. The dependence of Q and S_1 on the input variables $\boldsymbol{X}'$ is now modeled as

$$\boldsymbol{X}' = \begin{bmatrix} 1 & A & B & C & A \times B & A \times C & B \times C \end{bmatrix}^T, \tag{10}$$

$$\begin{aligned} Q' &= \boldsymbol{W}_Q{}^T \boldsymbol{X}', \\ S_1' &= \boldsymbol{W}_S{}^T \boldsymbol{X}', \end{aligned} \tag{11}$$

where $\boldsymbol{W}_Q$ is the coefficient vector of the regression model Q' and $\boldsymbol{W}_S$ is the coefficient vector of the regression model S_1'.

The prediction accuracy of the regression model is evaluated using the residual error (e_r) and average error (e_a), which are defined as

$$e_r = h_i - y_i, \tag{12}$$

$$e_a = \frac{\sum_{i=1}^{n} \frac{|e_{ri}|}{y_i} \times 100\%}{n}, \tag{13}$$

where h_i is the regression model predictive value, y_i is the reference value, and n is the number of data sets. To verify the prediction accuracy, nine groups of finite element calculations are carried out as a reference, which are compared with the output of Eq. (11). The errors are calculated from Eqs. (12) and (13), and e_r and e_a are shown in Table 3. It can be seen that the prediction errors for

Table 3
Prediction error of the regression model.

No.	Q/C^{-12}		$S_1 \times 100\%$	
	e_r	e_a	$e_r \times 10^{-3}$	e_a
1	−0.02		−1.79	
2	−0.90		−0.08	
3	1.53		5.42	
4	−1.31		−4.28	
5	0.57	0.75%	3.36	3.29%
6	−1.07		−1.37	
7	−0.17		−1.28	
8	0.32		0.77	
9	1.06		−0.74	

both Q and S_1 are regulated in a very small region, which indicates that the proposed regression models are accurate enough to construct the objective function.

4.2 Construction of first objective function

The first objective function is constructed from the two regression models Q' and S_1'. The entropy-CRITIC weighting is used to incorporate the influences of both the induced charge Q and location sensitivity S_1.

The first objective function is developed as

$$f = w_1 Q' + w_2 S_1', \tag{14}$$

$$F = -\left(w_1 Q' + w_2 S_1'\right), \tag{15}$$

where f is the first objective function and a large value is desirable. To simplify the optimization process, by negating f, the first objective function F is constructed as Eq. (15). In the optimization, the entropy weighting method (EW) is first used to determine the weight coefficient w_j'. Usually, there are correlations between different indexes that are not considered in EW. To solve this problem, the CRITIC weighting (CRITIC) is incorporated here to obtain the coefficient w_j'', in which the index variability and the correlation are considered. Then, w_j' and w_j'' are incorporated to generate the final weight coefficient w_j.

(1) Use EW to obtain w_j'

The original evaluation index matrix is normalized into a dimensionless non-negative standard matrix $\boldsymbol{R} = (r_{ij})_{m \times n}$,

$$\boldsymbol{R} = \begin{bmatrix} r_{11} & \cdots & r_{1n} \\ \vdots & r_{ij} & \vdots \\ r_{m1} & \cdots & r_{mn} \end{bmatrix}, \tag{16}$$

where i is the number of samples and j is the number of evaluation indexes.

The entropy value H_j is calculated from the standard matrix $\boldsymbol{R}$, which is defined as

$$H_j = -K\sum_{i=1}^{m} p_{ij} \ln p_{ij}, \begin{cases} K = (\ln m)^{-1} \\ p_{ij} = \dfrac{r_{ij}}{\sum_{i=1}^{m} r_{ij}} \end{cases} \quad j = 1, \cdots, n. \tag{17}$$

Then, w_j' of evaluation index j is calculated as

$$w_j' = \frac{1 - H_j}{\sum_{j=1}^{n} \left(1 - H_j\right)}. \tag{18}$$

(2) Use CRITIC to obtain w_j''

To consider the index variability, the standard deviation of the index is calculated as

$$\begin{cases} X_j = \dfrac{1}{n}\sum_{i=1}^{m} r_{ij}, \\ S_j = \sqrt{\dfrac{\sum_{i=1}^{m} (r_{ij} - X_j)^2}{m-1}}, \end{cases} \tag{19}$$

where X_j is the average of index j and S_j is the standard deviation. The correlation coefficient is calculated as

$$R_j = \sum_{i=1}^{n} (1 - R_{jk}), \tag{20}$$

where R_{jk} is the correlation coefficient between indexes j and k. The information given by the indexes is calculated using

$$C_j = S_j \times R_j, \tag{21}$$

where C_j is the information given by the jth index and R_j represents the linear correlation between indexes j and k. From Eqs. (20) and (21), the correlation coefficient w_j'' of index j is given by

$$w_j'' = \frac{C_j}{\sum_{j=1}^{n} C_j}. \tag{22}$$

(3) Incorporate w_j' and w_j'' to generate w_j

The above-mentioned nine groups of finite element calculation results are used here to compute coefficients w_j' and w_j'' from Eqs. (16)–(22), and the results are shown in Table 4. Then the final coefficients w_j used in Eqs. (14) and (15) are calculated as

$$w_j = \frac{w_j' w_j''}{\sum_{j=1}^{n} w_j' w_j''}. \tag{23}$$

4.3 Construction of second objective function

The manufacturing cost of the sensing array must be considered. To construct the cost objective function, several variables are defined here: the cost per element of the electronic device c_1, the cost of the PCB material per square meter c_2, the thickness processing fee per meter c_3, and the labor cost per element c_4. The second objective function *COST* is then built as follows:

$$COST = (c_1 + c_4)A + c_2 A \cdot B + c_3 A. \tag{24}$$

Here, the influence of factors A, B, and C on the two objective functions is investigated. The effect of the number of elements on the objective functions F and *COST* for 3, 4, and 5 elements is shown in Table 5. Conflicts can be observed for factors A and B but there is no conflict for factor C. Thus, here, we only consider the first two factors in the optimization.

$$\min \begin{cases} F(A,B) \\ COST(A,B) \end{cases} \tag{25}$$

Table 4
Calculation results of w' and w'' for indexes Q and S_1.

Evaluation index	H_j	EW coefficient w'	S_j	R_j	C_j	CRITIC coefficient w''
Q	0.8409	32.60%	0.09	1.294	0.116	45.09%
S_1	0.7897	43.08%	0.109	1.294	0.142	54.91%

Table 5
Effects of different factors on objective functions F and *COST*.

	A / element			B / $\times 10^{-4}$ m^2			C / $\times 10^{-4}$ m		
	3	4	5	3	4	5	3	4	5
$\|F\|$	58.87	68.29	77.71	58.87	67.31	75.75	58.87	46.42	33.98
COST	6.45	8.6	10.75	6.45	6.6	6.75	6.45	6.75	7.05
Analysis	Conflict			Conflict			No conflict		

4.4 Constraints

(1) Constraint of factor A

At least two electrode elements are required to form the array. The maximum number of electrodes is restricted by the installation space. To place the electronic devices and auxiliary circuit on the electrode, there is a minimum width requirement of 10 mm for the electrode, and this value is selected as the element width. The number of electrodes is maximum when there is no space interval angle between them. The constraint is expressed as

$$LB_a < A < UB_a,\ A \in N, \tag{26}$$

where LB_a is the lower limit and UB_a is the upper limit.

(2) Constraint of factor B

To place the circuit on the electrode surface, there is minimum area requirement for B. Also, since the electrode length must be less than the outer frame length of the sensor, the constraint for factor B can be expressed as

$$LB_b \le B \le UB_b,\ \ B \in 1\times10^{-5} N, \tag{27}$$

where LB_b is the lower limit and UB_b is the upper limit.

5. Optimization Design and Design Process of Electrode Array

In this section, the NSGA-II algorithm is employed to optimize the problem and the VIKOR method is used to select the final decision from the Pareto solution set.

5.1 Optimization algorithms

The NSGA-II method[21] is an evolutionary algorithm in which a population of candidate solutions evolves toward the best solution of a multi-objective optimization problem. The specific optimization procedure is shown in Fig. 11. First, the parent population P_t of N_{pop} individuals is initialized with uniform random values. Then, the offspring population Q_t is created after the crossover and mutation of P_t. The two populations P_t and Q_t are combined to form population R_t, and non-dominated sorting is performed on R_t to rank different fronts (F_i, i = 1, 2, …, etc.). Next, N_{pop} individuals are selected from R_t by sorting the crowding distance to create the next population P_{t+1}. This procedure can be iterated many times to provide the final result.

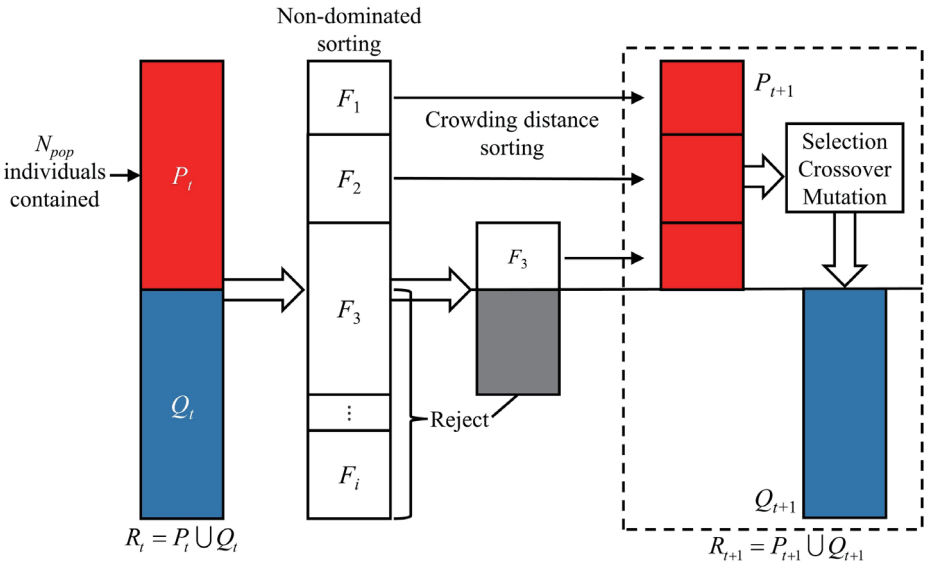

Fig. 11. (Color online) NSGA-II algorithm optimization procedure.

5.2 Decision-making of electrode array parameters

A decision based on the Pareto set must usually be made. VIKOR,[22] also known as the compromise ranking method, is an effective tool in multicriteria decision-making. First, the positive and negative ideal values are determined for different objectives. Then the maximum group benefit value S_i and the minimum individual regret value R_i are calculated for each individual in the Pareto set. Finally, the comprehensive evaluation value Q_i is calculated for each individual. The optimal individual can be selected on the basis of Q_i.

The corresponding negative ideal value (y^-) and positive ideal value (y^+) are determined as follows:

$$\begin{cases} y^- = (\max y_1(k), \max y_2(k), \cdots, \max y_m(k)), \\ y^+ = (\min y_1(k), \min y_2(k), \cdots, \min y_m(k)), \end{cases} (k = 1, 2, \cdots, n) \tag{28}$$

where n is the number of objective functions and m is the size of the Pareto set.

Then, w_k of each objective function is obtained by the EW. S_i and R_i are calculated for each individual as follows.

$$S_i = \left\{ \sum_{k=1}^{n} \left[w_k \frac{y^+(k) - y_i(k)}{y^+(k) - y^-(k)} \right]^2 \right\}^{\frac{1}{2}} \quad (i = 1, 2, \cdots, m) \tag{29}$$

$$R_i = \max_{1\le j\le n}\left(w_k \frac{y^+(k) - y_i(k)}{y^+(k) - y^-(k)}\right) \quad (i = 1, 2, \cdots, m) \tag{30}$$

Lastly, the comprehensive evaluation value Q_i is calculated as

$$\begin{aligned} &Q_i = v\frac{S^+ - S_i}{S^- - S^+} + (1-v)\frac{R^+ - R_i}{R^- - R^+}, \\ &S^+ = \max_{1\le i\le m} S_i, S^- = \min_{1\le i\le m} S_i, R^+ = \max_{1\le i\le m} R_i, R^- = \min_{1\le i\le m} R_i, \end{aligned} \quad (i = 1, 2, \cdots, m) \tag{31}$$

where v is the coefficient of the decision-making mechanism. When $v = 0.5$, it means that the decision-maker chooses a compromise to make decisions, in which the compromise mechanism can be fully used to minimize R_i and maximize S_i. A smaller value of Q_i means a higher priority in the selection.

6. Case Analysis

6.1 Optimization solution

In this section, the initial population number of the NSGA-II genetic algorithm is set to 20, the maximum number of iterations is 200, the crossover rate is 0.8, and the mutation rate is 0.05. The obtained Pareto set is shown in Fig. 12, in which the red dot represents the original scheme (A = 4, B = 0.00048, C = 0.0003) and the blue dots represent the optimized results. The 20 optimized solutions are shown in Table 6. It can be clearly seen from the optimization results that the optimized schemes are better than the original scheme.

6.2 Solution decision

VIKOR is used on the optimized schemes, and the decision results are shown in Fig. 13, in which the optimized schemes are listed from 1 to 20. Scheme 21 is the original scheme, for

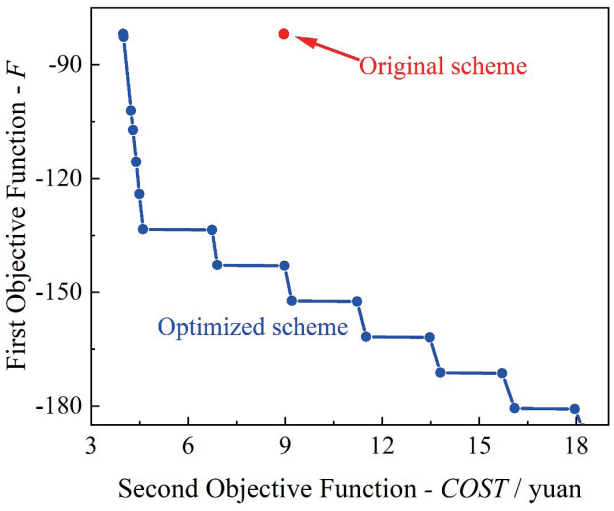

Fig. 12. (Color online) Pareto set.

Table 6
Optimized solutions for the electrode array design.

No.	Optimized scheme [*A*, *B*]	|*F*|	*COST*
1	[8, 0.001]	190.06	18.40
2	[2, 0.00039]	81.87	3.99
3	[2, 0.0004]	82.70	4.00
4	[8, 0.0095]	185.87	18.20
5	[8, 0.00089]	180.81	17.96
6	[4, 0.00089]	143.00	8.98
7	[6, 0.00089]	161.91	13.47
8	[5, 0.00089]	152.45	11.225
9	[3, 0.00089]	133.54	6.735
10	[7, 0.00089]	171.36	15.715
11	[3, 0.001]	142.83	6.90
12	[4, 0.001]	152.28	9.20
13	[7, 0.001]	180.62	16.10
14	[6, 0.001]	171.17	13.80
15	[2, 0.001]	133.38	4.60
16	[5, 0.001]	161.72	11.50
17	[2, 0.00079]	115.64	4.39
18	[2, 0.00063]	102.13	4.23
19	[2, 0.00089]	124.09	4.49
20	[2, 0.00069]	107.21	4.29

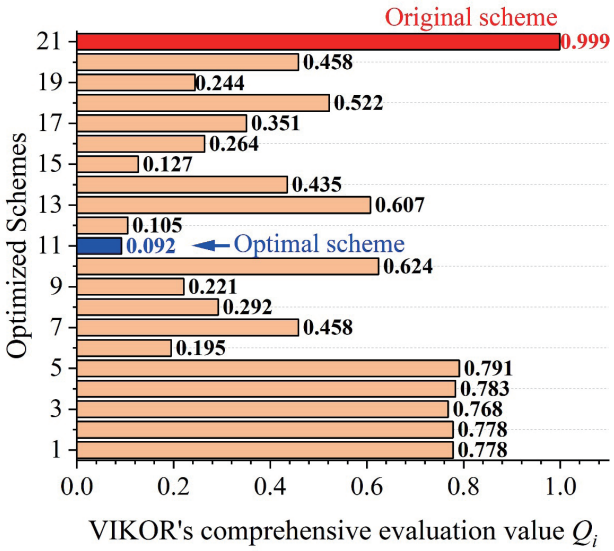

Fig. 13. (Color online) Decision of the optimized results.

which the absolute value of the first objective function is 81.92 and that of the second objective function is 8.96.

In Fig. 13, Q_i for each scheme is listed on the right of the bar graph. It can be seen that scheme 11, for which the absolute value of the first objective function is 142.83 and that of the second objective function is 6.90, is the optimal scheme. Compared with the original scheme, the first objective function value is increased by 74.35% and the second objective function value is decreased by 22.99%.

7. Conclusion

A multi-objective optimization method for non-invasive voltage sensors that considers the sensitivity, array arrangement, and cost is proposed in this paper. The total array induced charge Q and the location sensitivity S_1 are used to evaluate the sensor performance. Design criteria for the array arrangement based on these evaluation indexes are proposed, which include the electrode shape, the array profile, and the space interval angle between electrode elements. On the basis of the design criteria, two objective functions corresponding to the overall sensing performance and the manufacturing cost for the array design are investigated. The NSGA-II algorithm is employed to optimize the problem and the VIKOR strategy is finally used to select the decision from the Pareto set. Optimization results show that a rectangular shape is most suitable for the single electrode element, the sensing array is best designed in a ring profile, and the optimal number of electrodes is 3.

Acknowledgments

This work was partly supported by the Key R&D Project of Zhejiang Province under Grant 2021C0104, the Basic Industrial Science and Technology Project of Wenzhou under Grant G20210020, the Graduate Scientific Research Foundation of Wenzhou University under Grant 316202101057, the Natural Science Foundation of Zhejiang Province of China under Grant LGG20E070005, and the Major Science and Technology Project of Wenzhou under Grant ZG2021026.

References

1 B. Spencer Jr, M. E. Ruiz-Sandoval, and N. Kurata: Struct. Control Health Monit. **11** (2004) 349. http://doi.org/10.1002/stc.48
2 D. Lawrence, J. S. Donnal, S. Leeb, and Y. He: IEEE Sens. J. **16** (2016) 8990. http://doi.org/10.1109/JSEN.2016.2619666
3 S. Li, W. Peng, Q. Zhou, and X. Hou: 2019 IEEE Sustainable Power and Energy Conf. (IEEE, 2019) 2704–2707. https://doi.org/10.1109/iSPEC48194.2019.8974904
4 I. A. Metwally: IEEE Trans. Instrum. Meas. **59** (2009) 2211. https://doi.org/10.1109/TIM.2009.2030928
5 G. Can, W. Jingang, Y. Mengting, P. Hu, and M. Jun: Can. J. Appl. Sci. **14** (2014) 1030. https://doi.org/10.3923/jas.2014.1030.1036
6 D. Balsamo, D. Porcarelli, L. Benini, and B. Davide: Sensors, 2013 (IEEE, 2013) 1. https://doi.org/10.1109/ICSENS.2013.6688560
7 J. Wang, C. Gao, and J. Yang: Sensors **14** (2014) 12771. https://doi.org/10.3390/s140712771
8 K. Tsang and W. L. Chan: Sens. Actuators, A **167** (2011) 261. https://doi.org/10.1016/j.sna.2011.02.019
9 Y. Leng, L. Shu, Q. Qian, C. Chen, and Y. Lin: Sens. Mater. **34** (2022) 1057. https://doi.org/10.18494/SAM3848
10 X. Yan, J. Wang, P. Zhao, Z. Shen, X. Li, and R. Zhang: IEEE Trans. Instrum. Meas. **70** (2021) 1. https://doi.org/10.1109/TIM.2021.3073444
11 G. Geng, J. Wang, K.-L. Chen, and W. Xu: IEEE Trans. Instrum. Meas. **66** (2017) 2627. https://doi.org/10.1109/TIM.2017.2711898
12 D. J. Chmielewski, T. Palmer, and V. Manousiouthakis: AIChE J. **48** (2002) 1001. https://doi.org/10.1002/aic.690480510
13 S. Feng and J. Jia: Struct. Health Monit. **17** (2018) 169. https://doi.org/10.1177/1475921716688372
14 L. Wang, X. Wang, and X. Li: Eng. Comput. **33** (2016) 1070. https://doi.org/10.1108/EC-04-2015-0103
15 J. Wang, S. Law, and Q. Yang: J. Sound Vib. **333** (2014) 2469. https://doi.org/10.1016/j.jsv.2013.12.014
16 K. Kuang, M. Maalej, and S. Quek: J. Intell. Mater. Syst. Struct. **17** (2006) 361. https://doi.org/10.1177/1045389X06056339

17 R. T. Marler and J. S. Arora: Struct. Multidiscip. Optim. **26** (2004) 369. https://doi.org/10.1007/s00158-003-0368-6
18 T.-H. Yi, H.-N. Li, M. Gu, and X.-D. Zhang: Int. J. Struct. Stab. Dyn. **14** (2014) 1440012. https://doi.org/10.1142/S0219455414400124
19 Y. Tan and L. Zhang: Struct. Health Monit. **19** (2020) 1287. https://doi.org/10.1177/1475921719877579
20 C. Yang, X. Zhang, X. Huang, Z. Cheng, X. Zhang, and X. Hou: Acta Astronaut. **140** (2017) 213. https://doi.org/10.1016/j.actaastro.2017.08.025
21 K. Deb, A. Pratap, S. Agarwal, and T. Meyarivan: IEEE Trans. Evol. Comput. **6** (2002) 182. https://doi.org/10.1109/4235.996017
22 J. R. San Cristóbal: Renewable Energy **36** (2011) 498. https://doi.org/10.1016/j.renene.2010.07.031